

# Spontaneous Takeoff of Single Sulfur Nanoparticles during Sublimation Studied by Dark-Field Microscopy

Shasha Liu, Haoran Li, Susu Fang, Weigao Xu, Wenbing Hu,\* and Wei Wang\*



Cite This: *J. Am. Chem. Soc.* 2023, 145, 3987–3993



Read Online

ACCESS |



Metrics & More

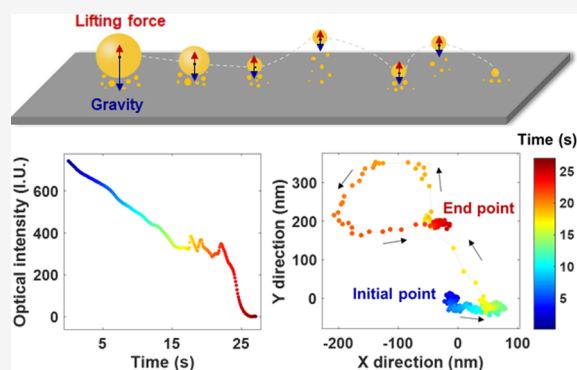


Article Recommendations



Supporting Information

**ABSTRACT:** The Leidenfrost effect describes a fascinating phenomenon in which a liquid droplet, when deposited on a very hot substrate, will levitate on its own vapor layer and undergo frictionless movements. Driven by the significant implications for heat transfer engineering and drag reduction, intensive efforts have been made to understand, manipulate, and utilize the Leidenfrost effect on macrosized objects with a typical size of millimeters. The Leidenfrost effect of nanosized objects, however, remains unexplored. Herein, we report on an unprecedented Leidenfrost effect of single nanosized sulfur particles at room temperature. It was discovered when advanced dark-field optical microscopy was employed to monitor the dynamic sublimation process of single sulfur nanoparticles sitting on a flat substrate. Despite the phenomenological similarity, including the vapor-cushion-induced levitation and the extended lifetime, the Leidenfrost effect at the nanoscale exhibited two extraordinary features that were obviously distinct from its macroscopic counterpart. First, there was a critical size below which single sulfur nanoparticles began to levitate. Second, levitation occurred in the absence of the temperature difference between the nanoparticle and the substrate, which was barely possible for macroscopic objects and underscored the value of bridging the gap connecting the Leidenfrost effect and nanoscience. The sublimation-triggered spontaneous takeoff of single sulfur nanoparticles shed new light on its further applications, such as nanoflight.



## INTRODUCTION

When a liquid droplet is placed on a hot solid with a temperature much higher than the boiling point of the liquid, in contrast to rapid disappearance due to intensive boiling as one would intuitively expect, film boiling at the solid–liquid interface generates a vapor cushion to levitate the droplet from the substrate.<sup>1,2</sup> The vapor cushion is fascinating because it not only results in thermal isolation to effectively decrease the heat transfer to a large extent and dramatically extend the lifetime of the droplet but also creates zero adhesion to enable beautiful and frictionless motion behaviors such as gliding,<sup>2</sup> self-propulsion,<sup>3</sup> rotation,<sup>4</sup> trampolining,<sup>5,6</sup> bouncing,<sup>7,8</sup> explosion,<sup>9</sup> and so on. This phenomenon is commonly known as the Leidenfrost effect to honor Johann Gottlob Leidenfrost, who made the first detailed documentation in 1756.

Driven by both fundamental and practical interests and enabled by modern measurement techniques and theoretical advancements, past decades have witnessed intensive revisits of the Leidenfrost effect.<sup>10</sup> From a fundamental point of view, the Leidenfrost effect provides an ideal interface to investigate the transition from nucleate boiling to film boiling and to better understand the fluid mechanics under frictionless conditions. More importantly, the Leidenfrost effect holds promising keys to many important industrial applications. For instance, engineering the hydrophobicity, roughness, and wettability of

solid surfaces via structural microtexturing allowed for tuning the Leidenfrost point by hundreds of degrees,<sup>11</sup> with implications for cooling and thermal management in steel and aerospace industry, combustion, and nuclear plants.<sup>12</sup> Rational fabrication of asymmetrical surface microstructures was proven an efficient way to design micromotors and actuators by harvesting the energy produced in the frictionless movements of objects.<sup>3,13</sup> The temperature gradient and the corresponding charge separation have been utilized in the chemical synthesis of functional nanomaterials.<sup>14,15</sup> In addition to the original Leidenfrost effect, where the vapor cushion was produced from the evaporation of liquid droplets, multiple variations have been proposed to expand the mechanisms for generating the vapor cushion, including the evaporation of hydrogels,<sup>8</sup> the sublimation of solid objects like dry ice,<sup>3</sup> and the evaporation or sublimation of the cold surface (like liquid

Received: October 11, 2022

Published: February 10, 2023



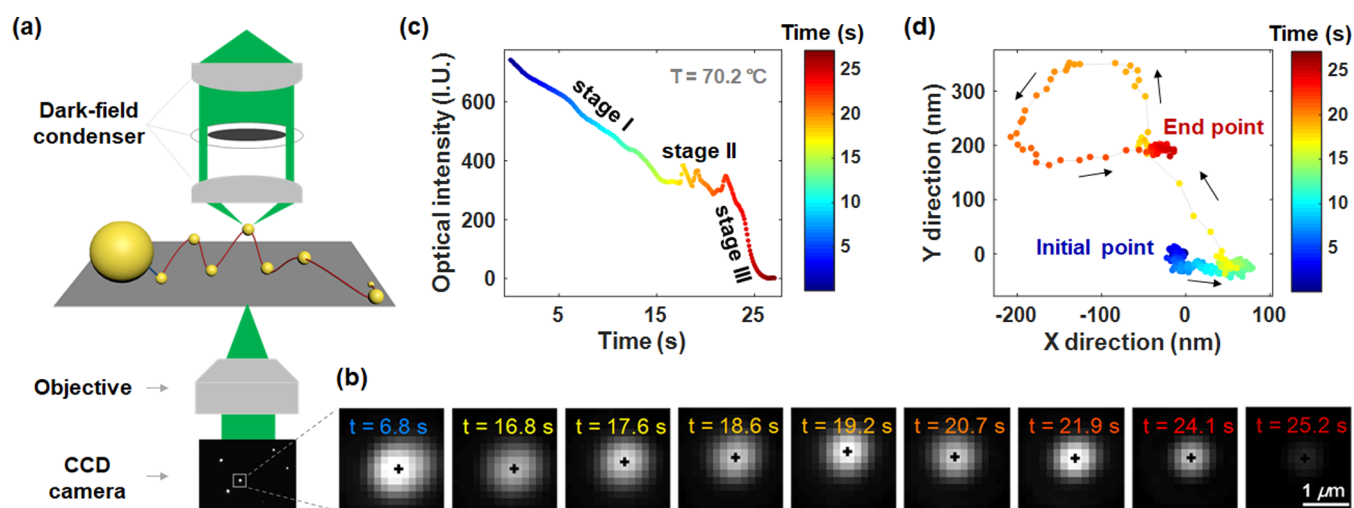


**Figure 1.** Optical imaging of the dynamic sublimation process of single sulfur nanoparticles. (a) Schematic illustration of monitoring the dynamic sublimation process of a single SNP with DFM. (b) Selected snapshots of one SNP from the time-lapsed DFM images during the entire sublimation process. The scale bar is  $1\ \mu\text{m}$ . (c, d) DFM intensity curves (c) and the location (d) as a function of the time of the SNP shown in panel (b), and the color of the points represent the moment of recording the images according to the time map shown on the right.

nitrogen or dry ice) when interacting with room temperature objects.<sup>13,16–18</sup>

Although successful, existing studies on the Leidenfrost effect have been exclusively performed on bulk objects with typical size in the millimeter scale. One then wonders whether the Leidenfrost effect also exists in a nanosized droplet or if it is only applicable on the macroscale. This question is particularly attractive because the interplay between nanoscience and the Leidenfrost effect has been rather weak despite the amazing achievements in nanoscience and nanotechnology in the past decades. When the size of the materials was reduced to the nanoscale, extraordinary properties arose and new phenomena were frequently observed.<sup>19</sup> Leidenfrost effect relies on various phase transitions and molecular interactions including evaporation, sublimation, surface tension, heat transfer, and friction, which are all size-dependent. For instance, numerous studies have demonstrated the great impact of object size on its surface tension and phase transition.<sup>20,21</sup> Molecular dynamics simulations have been employed to study the evaporation process of the nanodroplets, and the Leidenfrost temperature for water nanodroplets was found to be about 100 K lower than that of microdroplets.<sup>22</sup> In addition, gravity, another key player in levitation, also scales down as a power factor of 3 with the decreasing diameter, which greatly reduces the lifting force required to levitate the object and may have a significant impact on the nanoscale Leidenfrost effect. Celestini et al. discovered that the Leidenfrost droplet would takeoff from the plate as its size (weight) becomes small enough.<sup>23</sup> However, except for the promising theoretical study in a recent work,<sup>22</sup> to the best of our knowledge, the Leidenfrost effect of the nanosized object remains experimentally unexplored, likely due to the insufficient resolutions of major techniques (video camera and interferometry imaging) to monitor the motions of submicron objects and to characterize the nanoscale gap between the object and the substrate.

Here, we employed dark-field optical microscopy (DFM) to monitor the dynamic sublimation process of single sulfur nanoparticles (SNPs) sitting on a flat substrate under an ambient atmosphere at a constant temperature well below the

melting point of sulfur. In the early stage, the gentle sublimation induced a gradual decrease in the overall size of sulfur particles. When the particle size was below a critical value of  $\sim 360\ \text{nm}$ , it started to levitate, as evidenced by the stochastic movements and the transient increases in the particle–substrate distance, accompanied by the dramatically reduced sublimation rate and the extended lifetime of the particle. The critical size was dependent on the balance between the gravity of a single nanoparticle and the upward pressure caused by the dynamically accumulated sulfur vapors in the confined space underneath the nanoparticle. Both the vapor-cushion-induced levitation and the extended lifetime were nicely consistent with the characteristic features associated with the Leidenfrost effect. Despite the similarity, the Leidenfrost effect of single nanoparticles indeed exhibited two extraordinary features that were obviously distinct from the conventional experiments in millimeter-sized objects. First, for the same kind of sublimative materials, all individuals displayed a constant critical size for the levitation to occur regardless of their different original sizes. Comparative studies on single iodine and ferrocene particles indicated that the critical size was mostly dependent on the vapor pressure and density of the material. Second, the Leidenfrost effect of a single nanoparticle could occur even when there is no temperature difference between the particle and the substrate, a feature that has been barely possible for macroscopic objects.

## RESULTS AND DISCUSSION

**Optical Imaging of the Dynamic Sublimation Process of Single Sulfur Nanoparticles.** Figure 1a shows the schematic diagram of the experimental set-up, where a home-built DFM was employed to image the dynamic sublimation process of SNPs. A green light-emitting diode (LED) beam ( $\lambda = 520 \pm 30\ \text{nm}$ ) passed through the condenser and then illuminated the SNPs obliquely with an incident angle ranging from  $53.1^\circ$  to  $71.8^\circ$ . The photons scattered by the SNPs were subsequently collected by a  $20\times$  objective, while those photons directly transmitted through the background area without particles cannot enter the objective because the numerical aperture (N.A.) of the objective (0.45)

was smaller than that of the condenser (0.80–0.95). Therefore, a typical DFM image where SNPs were bright with high contrast to the dark background was obtained in the camera. Each bright dot in the DFM image represented a single SNP, and the optical intensity (brightness) of the dot was dependent on the number of atoms of the individual nanoparticle according to the light scattering theory,<sup>24</sup> laying the foundation for monitoring the dynamic sublimation of SNPs with DFM. With further calibration, the size of SNPs could be estimated from its DFM optical intensity, and the detection limit of this optical set-up was assessed to be 50 nm SNPs (Figure S1), which was determined by the contrast between the brightness of single SNPs and the spatial noise of its surrounded background.

In a typical experiment, the SNPs were first deposited on the substrate with a density of  $\sim 1$  particle/ $100 \mu\text{m}^2$ . Then, the time-lapsed DFM images were continuously recorded at a rate of 10 frames/s until all of the particles disappeared from the view (due to spontaneous sublimation). The temperature of the substrate was controlled by the Joule heating effect from a fabricated gold film underneath the SNPs (for more details, refer to Figure S2 and our previous work<sup>25</sup>) and kept at a constant temperature (70.2 °C) that was significantly lower than the melting temperature of bulk sulfur (115 °C)<sup>26</sup> during the whole recording process, as will be discussed in detail later. The photothermal effect of the illumination beam herein could be neglected because of its low power density ( $0.1 \mu\text{W}/\mu\text{m}^2$ ).<sup>27</sup> Figure 1b shows several DFM snapshots of one typical SNP in an experiment, where the scattering intensity of the SNP decreased with time, indicating that the sulfur atoms gradually escaped from the particle into air, i.e., sublimation. To further investigate the sublimation kinetics, its optical intensity curve as a function of time was extracted from a series of time-lapsed DFM images using home-written MATLAB codes (Figure 1c). Three-stage sublimation kinetics of the SNP were typically observed, including an early gentle sublimation stage I (0–15.6 s), a subsequent sublimation plateau stage II (15.6–23.1 s), and a final accelerated sublimation stage III (23.1–26.2 s). The slow sublimation of the initial large SNP and the rapid sublimation of the final small SNP were expected, which were consistent with the results of the sublimation of Ag nanoparticles and GeTe nanowires studied by transmission electron microscopy (TEM),<sup>28,29</sup> validating the feasibility of using the DFM to study the sublimation dynamics of single SNPs. Further studies indicated that the observed sublimation dynamic of single SNPs was not affected by the wavelength of illumination light used in the DFM and was an intrinsic property of the material (Figure S3). In contrast to the high vacuum in TEM, the atmospheric environment of the DFM makes it very suitable for characterizing the materials with high saturation vapor pressure, such as the sublimative sulfur herein. However, the intermediate sublimation stagnation stage II (i.e., the plateau in the time-dependent optical intensity curves) was observed for the first time.

In addition to the decrease in the optical intensity of the SNPs during the sublimation process, their position also appeared to change and displayed gliding behaviors by introducing a super-localization strategy to analyze the spatial movement of the SNPs (Figure 1b). When using a two-dimensional Gaussian function to fit the obtained DFM pattern (“bright dot”) of SNPs, the optical centroid of the pattern, i.e., the position of the particle, can be extracted

accurately (Figure S4). Such a super-localization strategy has been popularly used in tracking the movement trajectory of single nanoparticles,<sup>30</sup> resolving the electrochemical conversion process of single dielectric AgX nanoparticles,<sup>31</sup> and even mapping the reactivity hotspots of single TiO<sub>2</sub> nanorods.<sup>32</sup> An additional 2.5 $\times$  zoom-in lens was placed in front of the camera to further improve the magnification of optical imaging as well as the precision of the determining position of SNPs, and the positioning precision can reach 1 nm in this system (Figure S5). The black plus sign in each snapshot illustrates the obtained location of the particle at each moment. Plotting the location of the SNPs in a time sequence yields their trajectory during the sublimation process (Figure 1d). Note that the drift of the optical imaging system has been precorrected using a post-recording pixel reconstruction approach that we previously developed.<sup>33</sup> Moreover, adjacent individuals in the same field of view exhibited rather different trajectories, thus excluding the influence of environmental disturbance such as drift of stage (Figure S6).

The SNP moved over a distance of 500 nm, which was even greater than the size of the particle itself ( $d < 400$  nm), further excluding the possibility that the change in position was brought by spatially inhomogeneous sublimation of the particle. More importantly, when the position of the SNP was further correlated with its optical intensity by time, it was found that the significant motion of the SNP mainly occurred in stage II, when the optical intensity of the SNP was almost constant. The significantly reduced sublimation rate of SNPs, accompanied by the random movements, was nicely consistent with two characteristic features of the Leidenfrost effect. A movie is provided in the Supporting Information to deliver a comprehensive picture of the dynamic sublimation of the SNPs (Movie S1). These results indicated that the SNPs would levitate on the substrate and become a Leidenfrost nanoparticle at a certain moment during the sublimation.

Next, the time-dependent optical curves of all 31 SNPs in the field of view are shown in Figure 2a (left). It is interesting to find that not only is there a plateau (sublimation stagnation stage II) in the response of each particle, but the height of the plateau is essentially the same for the particles with different original optical intensities (sizes). Further, the optical intensity distribution of all points (4336 points) in the 31 curves was mapped (Figure 2a, right), and the high occurrence frequency of points with an optical intensity of  $\sim 320$  IU was also clearly observed, verifying the long duration of the SNPs with a critical size during the sublimation process. In other words, the SNPs will be levitated and stop sublimation when their size drops to a constant critical value regardless of their original size, which is obviously distinct from the conventional Leidenfrost effect in millimeter-sized objects. As the substrate temperature further decreased, similar sublimation dynamics were observed and the sublimation rate was reduced. In addition, the lifetime of the plateau stage II became significantly longer (Figure S7), which was consistent with the classic Leidenfrost effect on the microscale droplets.<sup>34</sup> Interestingly, even at room temperature, the levitation of SNPs still occurred at the same critical size within a significantly extended recording time of a few hours (Figure 2b). Note that there was no temperature difference between the SNPs and the substrate. This feature has been barely possible in the conventional Leidenfrost effect on macroscopic objects. To further examine the influence of the substrate on the phenomenon, a 40 nm thick layer of SiO<sub>2</sub> was sputtered on

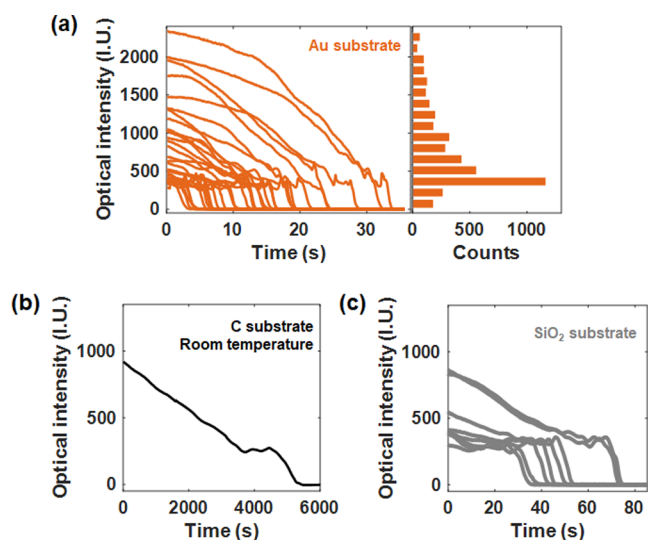


**Figure 2.** Sublimation kinetics of single SNPs under different conditions. The time-dependent DFM intensity curves of (a) 31 SNPs on the Au substrate with a temperature of 70.2 °C, (b) one SNP on the carbon substrate at room temperature, and (c) eight SNPs on the SiO<sub>2</sub> substrate with a temperature of 61.8 °C, respectively. And the histogram (a, right) counts the occurrence frequency of the optical intensity of all data points that existed in the 31 curves of panel (a) (left).

the surface of the previously used Au film (Figure S8). Similar sublimation kinetics and critical size were found on both SiO<sub>2</sub> and Au substrates (Figure 2c), suggesting that the substrate solely acted as a surface to support the SNPs and did not exhibit specific interactions with SNPs or sulfur vapors.

**Raman Characterization of the Single Sulfur Nanoparticles During the Sublimation.** Along with the quantitative optical measurement, the dynamic chemical composition of a single SNP throughout the sublimation process was also characterized by a confocal micro-Raman spectrometer. The time-lapsed Raman spectra of a single SNP during the entire sublimation process are shown in Figure 3a, where the particle kept the characteristic peak of  $\alpha$ -S<sub>8</sub> until its disappearance,<sup>35,36</sup> verifying that the change in the DFM optical intensity as well as the location was only brought by the sublimation of SNPs. It has been well-documented that liquid sulfur displayed a wing feature in the low-frequency range (10–100 cm<sup>-1</sup>, Boson peak) due to the disorder of molecules

in the liquid.<sup>36</sup> The absence of such a band clearly excluded the phase transition from solid to liquid, i.e., melting of sulfur, which validated the nature of sublimation. Further results clearly exhibited the different response between melting and sublimation of single sulfur particles in Raman microscopy as well as in DFM (Figure S9). Moreover, the intensity of the Raman scattering is also related to the amount of sulfur–sulfur bonds and thus the size of the SNPs. Taking the peak intensity of 153 cm<sup>-1</sup> as an example (representing the asymmetric S–S bending vibrational modes), a similar plateau was also observed in the curve of time-dependent Raman intensity (inelastic scattering, Figure 3b), providing independent validation of the DFM results (elastic scattering).

A hypothetical scenario was finally proposed to describe the Leidenfrost effect in the sublimative nanoparticles with a critical size at room temperature (Figure 4a). During the sublimation, the sulfur molecules escaping from the solid SNPs efficiently diffuse into the air in all directions. However, due to the existence of the substrate, a portion of the escaped sulfur molecules are trapped in the confined space between SNPs and the substrate. The accumulated sulfur molecules further form a vapor layer and exert an upward force on the SNPs. The lifting force is determined by the saturated vapor pressure of the sulfur, which is relatively constant throughout the sublimation process, while the gravity of SNPs gradually decreases as sublimation proceeds. Hence, when the gravity of SNP decreases to a critical point that is equal to the lifting force provided by the vapor layer underneath the nanoparticle, the SNP starts to levitate and takeoff. A similar explanation has been proposed by Celestini et al. to understand the takeoff behavior of the Leidenfrost droplets from the substrate when its radius decreased to a critical size.<sup>23</sup> The takeoff is also determined by the balance of the weight and upward pressure provided by the vapor layer between the droplets and the substrate. Further, it was found that the critical size became larger after increasing the sulfur vapor concentration of the system (Figure S10), verifying that the sulfur vapor herein plays an important role in the takeoff of the SNP by balancing its gravity.

The as-used DFM is a far-field imaging technique with a depth of focus of about 5  $\mu$ m. This feature makes it difficult to detect the vertical movement of SNPs along the Z direction, although it is very sensitive to the movement of the SNPs in the X–Y direction (Figure 1b). To resolve the transient and small changes in the SNP–substrate vertical distance during

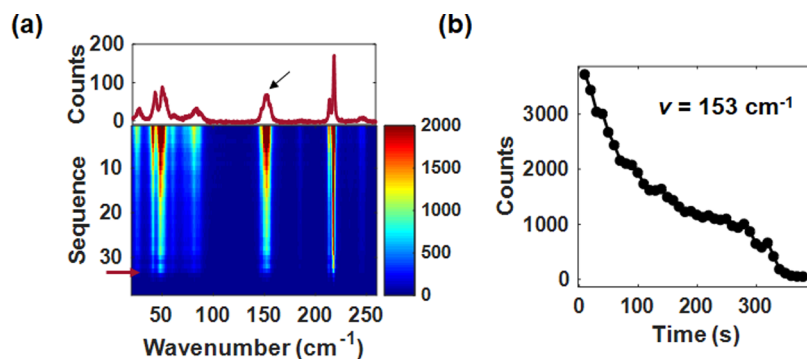


**Figure 3.** Raman characterization results of the single sulfur nanoparticles during the sublimation. (a) Time-dependent Raman spectra of one SNP during the sublimation process (in a pseudo color map format) and one of the typical Raman spectra of SNPs indicated by the red arrow was shown in the upper inset. The acquisition time of each spectrum is 10 s. (b) Time-dependent Raman intensity curve of 153 cm<sup>-1</sup> peaks (indicated by the black arrow in panel (a)) of the SNPs during the sublimation process.

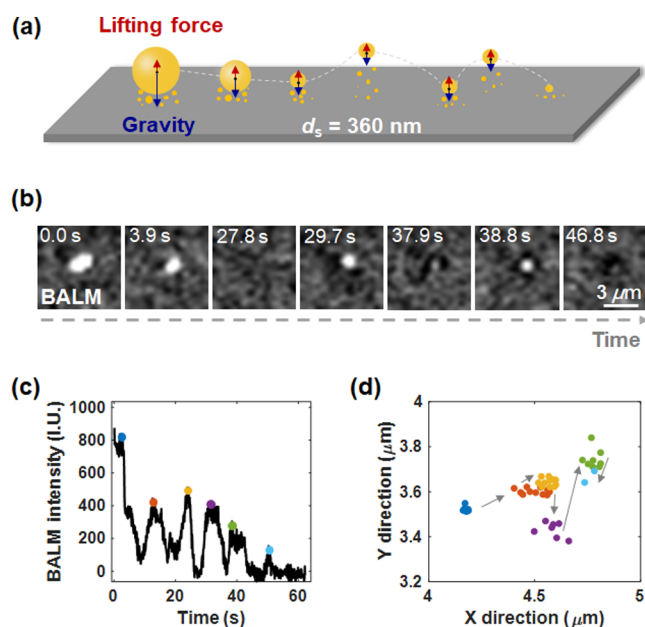


**Figure 4.** Description and confirmation of the hypothetical scenario of the Leidenfrost effect in the sublimative nanoparticles. (a) Schematic illustration of proposed hypothesis scenario to explain the observed Leidenfrost effect in single sublimative nanoparticles. (b) Selected snapshots of one SNP from the time-lapsed BALM images during the entire sublimation process. (c) BALM intensity curve of the SNP shown in panel (b) as a function of time. (d) Location of the SNP at the moment indicated by color dots in panel (c).

levitation and movements, another recently developed nanoscale optical imaging technique that has single nanoparticle sensitivity and sub-nanometer-scale vertical resolution on sensing the local refractive index change at the surface,<sup>37,38</sup> termed backside absorption layer microscopy (BALM), was then employed to monitor the sublimation process of the SNPs (Figure 4b). BALM was based on the destructive interference between the light reflected by two surfaces of a properly absorbing layer. The optical intensity of the SNPs in BALM is determined not only by their size but also by the distance between the SNPs and substrate (Figure S11). Accompanying the movement of SNPs in the X–Y direction, an obvious blinking in the optical intensity of the SNPs was simultaneously observed in BALM (Movie S2). After the SNP completely disappeared from the optical image for a few seconds, it reappeared in the camera, and its optical intensity recovered to that before its disappearance (Figure 4b,c). Since the size of the SNPs decreased monotonically during the sublimation process, the large fluctuations in the optical trajectory were mostly contributed by the periodic fluctuations in the vertical distance, i.e., bouncing. In addition, the position of the SNP significantly changed in the reciprocal of its disappearance and reappearance (Figure 4d). These results provided vivid evidence for the conjecture that SNPs below the critical size would be lifted and undergo frictionless movements.

Lastly, the critical size for the SNPs to levitation was assessed. One classical method for determining the critical size is to directly characterize the SNPs in the Leidenfrost state by scanning electron microscopy (SEM), which has a higher spatial resolution than optical microscopy. However, due to the rapid sublimation of sulfur under the high vacuum environment of SEM,<sup>35</sup> it is difficult to accurately determine the real

size of the Leidenfrost sulfur nanoparticles. Therefore, the critical size herein for the Leidenfrost sulfur nanoparticles was optically calibrated by the standard SiO<sub>2</sub> nanospheres with known size, which was determined to be about 360 nm according to the light scattering theory (for more details, refer to Figure S12). For ease of estimation, we assume that the shape of sulfur is spherical. Hence, the mechanical equilibrium  $P_s = Mg$  can be further written as  $P\pi r^2 = 4/3\pi r^3\rho g$ , and it occurs when the vapor pressure reaches an order of  $P = 4/3\rho gr$ . By substituting the critical radius  $r = 180$  nm, the magnitude of the vapor pressure  $P$  required to lift the Leidenfrost SNPs is about 5.5 mPa, which is equivalent to the vapor pressure of sulfur at  $\sim 48$  °C according to its phase diagram.<sup>35,41</sup> It is worth noting that the estimation herein is oversimplified, but the estimation should be considered to support the argument that the observed critical size was in the reasonable range for sulfur. This estimation was further supported by the response of more species with a higher vapor pressure. Similar takeoff behaviors were also observed in the sublimation process of the single iodine and ferrocene particles. Moreover, it was found that the average critical size increased with the ratio of the vapor pressure to the density of the species (Figure 5). These further results not only revealed

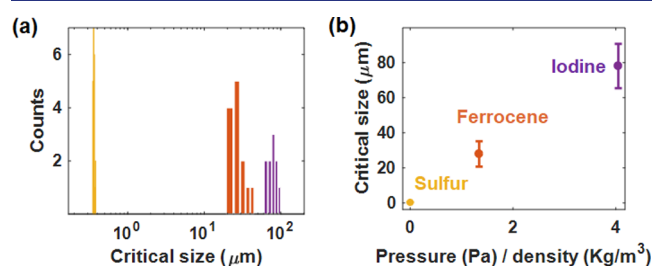


**Figure 5.** Statistical analysis of the critical size of different sublimative species. (a) Critical size of iodine with a vapor pressure of 20 Pa (purple bars),<sup>39</sup> ferrocene with a vapor pressure of 1 Pa (orange bars),<sup>40</sup> and sulfur with a vapor pressure of 5 mPa (yellow bars).<sup>35</sup> (b) Linear dependence of the critical size on the ratio between the vapor pressure and density of the different species shown in panel (a).

the generality of spontaneous takeoff of single sublimative particles during sublimation but also further verified the rationality of the hypothesis.

## CONCLUSIONS

In summary, the sublimation kinetics of single sulfur nanoparticles sitting on a flat substrate have been successfully studied by a home-built dark-field optical microscopy. The Leidenfrost effect is observed in the dynamic sublimation process of single nanoparticles for the first time, evidenced by the transient increases in the particle–substrate distance, dramatically reduced sublimation rate, and the random movement of the nanoparticles. In addition to the above characteristics that are similar to the classical Leidenfrost effect of bulk objects, there are two other unique features of the Leidenfrost effect that existed in the sublimable nanoparticles. (1) It emerges below a critical size, which is determined by the balance between the density and the vapor pressure of the nanoparticles. (2) It could happen at a temperature well below the melting temperature of the material, even occurring in the absence of the temperature difference between the nanoparticle and the substrate. This work not only uncovers the sublimation-triggered takeoff of a single sulfur nanoparticle

below a critical size, shedding new light on its application, but also develops a general methodology for directly studying the Leidenfrost effect at the nanoscale. We further foresee the applications of the present method in many other nanoparticles to dig out more attractive interplays between nanoscience and the Leidenfrost effect.

## METHODS

**Materials and Characterization.** Sulfur powder (1 mg) (Alfa Aesar) was first dispersed in 1 mL of deionized water (18.2 M $\Omega$ -cm). The obtained suspension was then sonicated for 1 min, and 5  $\mu$ L of the supernatant was dropped on the substrate. The phosphate buffer solution (5  $\mu$ L) was then used to accelerate the binding process of nanoparticles onto the substrate. When the nanoparticles sat on the substrate and reached an appropriate density, the suspension was removed and the nanoparticles were then washed with deionized water and finally dried in air. The iodine (Aladdin) and ferrocene (Aladdin) particles were directly sprinkled on the substrate. The Au substrate was fabricated by successively sputtering a 2 nm thick chromium adhesion layer and a 47 nm thick gold layer on the coverslip (Fisherbrand). The pattern of the gold film was fabricated by lithography. The SiO<sub>2</sub> substrate was produced by further sputtering a 40 nm thick SiO<sub>2</sub> layer on the Au substrate. The carbon substrate was made by simply sputtering 1 nm thick carbon on the coverslip. The SiO<sub>2</sub> nanospheres used for optical intensity calibration were purchased from Macklin, and the accurate size of the SiO<sub>2</sub> nanospheres was characterized by scanning electron microscopy (Phenom scientific).

**Apparatus.** Dark-field microscopy (DFM) was built based on commercial Ti2E microscopy. A dry condenser (N.A. = 0.95–0.80) focuses the illumination beam (white LED, Nikon, filtered by a 520/70 nm bandpass filter, Semrock) and limits the incident angle from 53.1 to 71.8°. A portion of the photons scattered by sulfur nanoparticles pass through the objective (Nikon, N.A. = 0.45) and are collected by a CCD camera (Pike F-032B, Allied Vision Technologies).

Backside absorbing layer microscopy (BALM) was also built based on inverted Ti2E microscopy. A green light beam served as the light source (mercury lamp, filtered by a 520/70 nm bandpass filter), which was first reflected by a 50–50 beam splitter (Thorlabs), followed by illuminating the sulfur particles from the backside. The particles sat on the substrate with a 10 nm thick Au film, and the reflected light was finally collected by the CCD (Pike F-032B, Allied Vision Technologies).

For confocal Raman microscopy (Horiba, LabRAM HR Evolution), a laser with a wavelength of 633 nm was used to illuminate the sulfur nanoparticles sitting on the Au substrate, and the light spot was converged to a size of 1  $\mu$ m<sup>2</sup> by a 100 $\times$  objective (Olympus, N.A. = 0.90). The Raman spectra of sulfur nanoparticles were continuously acquired, and the acquisition time for each spectrum was 10 s. Three BraggGrate notch filters (BNFs) were used to block the incident light, which enables the collection of low-frequency scattering signals down to 5 cm<sup>-1</sup>.

The temperature of the substrate was simply controlled by adjusting the electrical power applied to the Au film by an electrical workstation (CS120, Corrtest).

## ASSOCIATED CONTENT

### Supporting Information

The Supporting Information is available free of charge at <https://pubs.acs.org/doi/10.1021/jacs.2c10763>.

Detailed data analysis and supporting data (PDF)

Time-lapsed DFM images of the SNPs during a complete sublimation process (Movie S1) (AVI)

Time-lapsed BALM images of the SNPs during a complete sublimation process (Movie S2) (AVI)

## AUTHOR INFORMATION

### Corresponding Authors

**Wenbing Hu** – Department of Polymer Science and Engineering, School of Chemistry and Chemical Engineering, Nanjing University, Nanjing 210023, China; [orcid.org/0000-0002-7795-9004](https://orcid.org/0000-0002-7795-9004); Email: [wphu@nju.edu.cn](mailto:wphu@nju.edu.cn)

**Wei Wang** – State Key Laboratory of Analytical Chemistry for Life Science, Chemistry and Biomedicine Innovation Center (ChemBIC), School of Chemistry and Chemical Engineering, Nanjing University, Nanjing 210023, China; [orcid.org/0000-0002-4628-1755](https://orcid.org/0000-0002-4628-1755); Email: [wei.wang@nju.edu.cn](mailto:wei.wang@nju.edu.cn)

### Authors

**Shasha Liu** – State Key Laboratory of Analytical Chemistry for Life Science, Chemistry and Biomedicine Innovation Center (ChemBIC), School of Chemistry and Chemical Engineering, Nanjing University, Nanjing 210023, China; [orcid.org/0000-0002-0733-9694](https://orcid.org/0000-0002-0733-9694)

**Haoran Li** – State Key Laboratory of Analytical Chemistry for Life Science, Chemistry and Biomedicine Innovation Center (ChemBIC), School of Chemistry and Chemical Engineering, Nanjing University, Nanjing 210023, China; [orcid.org/0000-0001-8825-3069](https://orcid.org/0000-0001-8825-3069)

**Susu Fang** – Department of Polymer Science and Engineering, School of Chemistry and Chemical Engineering, Nanjing University, Nanjing 210023, China

**Weigao Xu** – Department of Polymer Science and Engineering, School of Chemistry and Chemical Engineering, Nanjing University, Nanjing 210023, China; [orcid.org/0000-0002-3014-756X](https://orcid.org/0000-0002-3014-756X)

Complete contact information is available at: <https://pubs.acs.org/10.1021/jacs.2c10763>

### Author Contributions

All authors have given approval to the final version of the manuscript.

### Notes

The authors declare no competing financial interest.

## ACKNOWLEDGMENTS

The authors thank the National Natural Science Foundation of China (Grants 21925403 and 21874070) and the Excellent Research Program of Nanjing University (Grant ZYJH004) for the financial support.

## REFERENCES

- (1) Burton, J. C.; Sharpe, A. L.; van der Veen, R. C. A.; Franco, A.; Nagel, S. R. Geometry of the Vapor Layer Under a Leidenfrost Drop. *Phys. Rev. Lett.* **2012**, *109*, No. 074301.
- (2) Quéré, D. Leidenfrost Dynamics. *Annu. Rev. Fluid Mech.* **2013**, *45*, 197–215.
- (3) Lagubeau, G.; Le Merrer, M.; Clanet, C.; Quéré, D. Leidenfrost on a ratchet. *Nat. Phys.* **2011**, *7*, 395–398.
- (4) Bouillant, A.; Mouterde, T.; Bourriane, P.; Lagarde, A.; Clanet, C.; Quéré, D. Leidenfrost wheels. *Nat. Phys.* **2018**, *14*, 1188–1192.
- (5) Graeber, G.; Regulagadda, K.; Hodel, P.; Küttel, C.; Landolf, D.; Schutzius, T. M.; Poulikakos, D. Leidenfrost droplet trampolining. *Nat. Commun.* **2021**, *12*, No. 1727.
- (6) Schutzius, T. M.; Jung, S.; Maitra, T.; Graeber, G.; Köhme, M.; Poulikakos, D. Spontaneous droplet trampolining on rigid superhydrophobic surfaces. *Nature* **2015**, *527*, 82–85.
- (7) Waitukaitis, S. R.; Zuiderwijk, A.; Souslov, A.; Coullais, C.; van Hecke, M. Coupling the Leidenfrost effect and elastic deformations to power sustained bouncing. *Nat. Phys.* **2017**, *13*, 1095–1099.

- (8) Pham, J. T.; Paven, M.; Wooh, S.; Kajiya, T.; Butt, H.-J.; Vollmer, D. Spontaneous jumping, bouncing and trampolining of hydrogel drops on a heated plate. *Nat. Commun.* **2017**, *8*, No. 905.
- (9) Lyu, S.; Mathai, V.; Wang, Y.; Sobac, B.; Colinet, P.; Lohse, D.; Sun, C. Final fate of a Leidenfrost droplet: Explosion or takeoff. *Sci. Adv.* **2019**, *5*, No. eaav8081.
- (10) Stewart, S. Leidenfrost drop dynamics: a forgotten past and modern day rediscoveries. *Eur. J. Phys.* **2022**, *43*, No. 023001.
- (11) Jiang, M.; Wang, Y.; Liu, F.; Du, H.; Li, Y.; Zhang, H.; To, S.; Wang, S.; Pan, C.; Yu, J.; Quéré, D.; Wang, Z. Inhibiting the Leidenfrost effect above 1,000 °C for sustained thermal cooling. *Nature* **2022**, *601*, 568–572.
- (12) Lyu, S.; Tan, H.; Wakata, Y.; Yang, X.; Law, C. K.; Lohse, D.; Sun, C. On explosive boiling of a multicomponent Leidenfrost drop. *Proc. Natl. Acad. Sci. U.S.A.* **2021**, *118*, No. e2016107118.
- (13) Wells, G. G.; Ledesma-Aguilar, R.; McHale, G.; Sefiane, K. A sublimation heat engine. *Nat. Commun.* **2015**, *6*, No. 6390.
- (14) Abdelaziz, R.; Disci-Zayed, D.; Hedayati, M. K.; Pöhls, J.-H.; Zillohu, A. U.; Erkartal, B.; Chakravadhanula, V. S. K.; Duppel, V.; Kienle, L.; Elbahri, M. Green chemistry and nanofabrication in a levitated Leidenfrost drop. *Nat. Commun.* **2013**, *4*, No. 2400.
- (15) Elbahri, M.; Abdelaziz, R.; Disci-Zayed, D.; Homaeigohar, S.; Sosna, J.; Adam, D.; Kienle, L.; Dankwort, T.; Abdelaziz, M. Underwater Leidenfrost nanochemistry for creation of size-tailored zinc peroxide cancer nanotherapeutics. *Nat. Commun.* **2017**, *8*, No. 15319.
- (16) Gauthier, A.; Diddens, C.; Proville, R.; Lohse, D.; van der Meer, D. Self-propulsion of inverse Leidenfrost drops on a cryogenic bath. *Proc. Natl. Acad. Sci. U.S.A.* **2019**, *116*, 1174–1179.
- (17) Antonini, C.; Bernagozzi, I.; Jung, S.; Poulikakos, D.; Marengo, M. Water Drops Dancing on Ice: How Sublimation Leads to Drop Rebound. *Phys. Rev. Lett.* **2013**, *111*, No. 014501.
- (18) Song, Y. S.; Adler, D.; Xu, F.; Kayaalp, E.; Nureddin, A.; Anchan, R. M.; Maas, R. L.; Demirci, U. Vitrification and levitation of a liquid droplet on liquid nitrogen. *Proc. Natl. Acad. Sci. U.S.A.* **2010**, *107*, 4596–4600.
- (19) Sun, J.; He, L.; Lo, Y.-C.; Xu, T.; Bi, H.; Sun, L.; Zhang, Z.; Mao, S. X.; Li, J. Liquid-like pseudoelasticity of sub-10-nm crystalline silver particles. *Nat. Mater.* **2014**, *13*, 1007–1012.
- (20) Bzdek, B. R.; Reid, J. P.; Malila, J.; Prisle, N. L. The surface tension of surfactant-containing, finite volume droplets. *Proc. Natl. Acad. Sci. U.S.A.* **2020**, *117*, 8335–8343.
- (21) Cheng, Y.; Su, H.; Koop, T.; Mikhailov, E.; Pöschl, U. Size dependence of phase transitions in aerosol nanoparticles. *Nat. Commun.* **2015**, *6*, No. 5923.
- (22) Rodrigues, J.; Desai, S. The nanoscale Leidenfrost effect. *Nanoscale* **2019**, *11*, 12139–12151.
- (23) Celestini, F.; Frisch, T.; Pomeau, Y. Take Off of Small Leidenfrost Droplets. *Phys. Rev. Lett.* **2012**, *109*, No. 034501.
- (24) Zhu, S.; Ma, L.; Wang, S.; Chen, C.; Zhang, W.; Yang, L.; Hang, W.; Nolan, J. P.; Wu, L.; Yan, X. Light-Scattering Detection below the Level of Single Fluorescent Molecules for High-Resolution Characterization of Functional Nanoparticles. *ACS Nano* **2014**, *8*, 10998–11006.
- (25) Liu, S.; Lv, M.; Li, H.; Wang, S.; Feng, C.; Wang, X.; Hu, W.; Wang, W. Optical Imaging of the Molecular Mobility of Single Polystyrene Nanospheres. *J. Am. Chem. Soc.* **2022**, *144*, 1267–1273.
- (26) Liu, N.; Zhou, G.; Yang, A.; Yu, X.; Shi, F.; Sun, J.; Zhang, J.; Liu, B.; Wu, C.-L.; Tao, X.; Sun, Y.; Cui, Y.; Chu, S. Direct electrochemical generation of supercooled sulfur microdroplets well below their melting temperature. *Proc. Natl. Acad. Sci. U.S.A.* **2019**, *116*, 765–770.
- (27) Liu, S.; Zhou, K.; Yuan, T.; Lei, W.; Chen, H.-Y.; Wang, X.; Wang, W. Imaging the Thermal Hysteresis of Single Spin-Crossover Nanoparticles. *J. Am. Chem. Soc.* **2020**, *142*, 15852–15859.
- (28) Asoro, M. A.; Kovar, D.; Ferreira, P. J. In situ Transmission Electron Microscopy Observations of Sublimation in Silver Nanoparticles. *ACS Nano* **2013**, *7*, 7844–7852.
- (29) Yim, J. W. L.; Xiang, B.; Wu, J. Sublimation of GeTe Nanowires and Evidence of Its Size Effect Studied by in Situ TEM. *J. Am. Chem. Soc.* **2009**, *131*, 14526–14530.
- (30) Feng, J.; Zhang, Z.; Wen, X.; Xue, J.; He, Y. Single Nanoparticle Tracking Reveals Efficient Long-Distance Undercurrent Transport in Upper Fluid of Bacterial Swarms. *iScience* **2019**, *22*, 123–132.
- (31) Lemineur, J.-F.; Noël, J.-M.; Courty, A.; Ausserré, D.; Combellas, C.; Kanoufi, F. In Situ Optical Monitoring of the Electrochemical Conversion of Dielectric Nanoparticles: From Multistep Charge Injection to Nanoparticle Motion. *J. Am. Chem. Soc.* **2020**, *142*, 7937–7946.
- (32) Sambur, J. B.; Chen, T.-Y.; Choudhary, E.; Chen, G.; Nissen, E. J.; Thomas, E. M.; Zou, N.; Chen, P. Sub-particle reaction and photocurrent mapping to optimize catalyst-modified photoanodes. *Nature* **2016**, *530*, 77–80.
- (33) Gao, J.; Wo, X.; Wang, Y.; Li, M.; Zhou, C.; Wang, W. Postrecording Pixel-Reconstruction Approach for Correcting the Lateral Drifts in Surface Plasmon Resonance Microscope. *Anal. Chem.* **2019**, *91*, 13620–13626.
- (34) Celestini, F.; Frisch, T.; Pomeau, Y. Room temperature water Leidenfrost droplets. *Soft Matter* **2013**, *9*, 9535–9538.
- (35) Levin, B. D. A.; Zachman, M. J.; Werner, J. G.; Sahore, R.; Nguyen, K. X.; Han, Y.; Xie, B.; Ma, L.; Archer, L. A.; Giannelis, E. P.; Wiesner, U.; Kourkoutis, L. F.; Muller, D. A. Characterization of Sulfur and Nanostructured Sulfur Battery Cathodes in Electron Microscopy Without Sublimation Artifacts. *Microsc. Microanal.* **2017**, *23*, 155–162.
- (36) Nims, C.; Cron, B.; Wetherington, M.; Macalady, J.; Cosmidis, J. Low frequency Raman Spectroscopy for micron-scale and in vivo characterization of elemental sulfur in microbial samples. *Sci. Rep.* **2019**, *9*, No. 7971.
- (37) Campidelli, S.; Khachfe, R. A.; Jaouen, K.; Monteiller, J.; Amra, C.; Zerrad, M.; Cornut, R.; Derycke, V.; Ausserré, D. Backside absorbing layer microscopy: Watching graphene chemistry. *Sci. Adv.* **2017**, *3*, No. e1601724.
- (38) Lemineur, J.-F.; Noël, J.-M.; Ausserré, D.; Combellas, C.; Kanoufi, F. Combining Electrodeposition and Optical Microscopy for Probing Size-Dependent Single-Nanoparticle Electrochemistry. *Angew. Chem., Int. Ed.* **2018**, *57*, 11998–12002.
- (39) Gillespie, L. J.; Fraser, L. H. D. The Normal Vapor Pressure of Crystalline Iodine. *J. Am. Chem. Soc.* **1936**, *58*, 2260–2263.
- (40) Edwards, J. W.; Kington, G. L. Thermodynamic properties of ferrocene. Part 2.—Vapour pressure and latent heat of sublimation at 25 °C by the effusion and thermistor manometer methods. *Trans. Faraday Soc.* **1962**, *58*, 1323–1333.
- (41) Ferreira, A. G. M.; Lobo, L. Q. The low-pressure phase diagram of sulfur. *J. Chem. Thermodyn.* **2011**, *43*, 95–104.